Spin-mixed doubly excited resonances in Ca and Sr spectra

J. H. Chen,[1] T. K. Fang,[2,*] C. C. Chu,[3] T. S. Yih,[3] and T. N. Chang[4]
[1]*Graduate Institute of Applied Science and Engineering, Fu Jen Catholic University, Taipei, Taiwan 242, Republic of China*
[2]*Department of Physics, Fu Jen Catholic University, Taipei, Taiwan 242, Republic of China*
[3]*Department of Physics, National Central University, Chungli, Taiwan 32054, Republic of China*
[4]*Department of Physics and Astronomy, University of Southern California, Los Angeles, California 90089-0484, USA*
(Received 18 August 2009; published 19 October 2009)

We present a joint theoretical and experimental investigation to demonstrate explicitly how the combined spin-dependent interaction and the configuration interaction may affect the mixing of different spin states along various doubly excited autoionization series for Ca and Sr as energy increases across several ionization thresholds. In particular, our study has identified the inversion of energy levels between members of a number of multiplets, i.e., in contrast to the Hund's rules, due to the presence of perturber from other overlapping resonance series. We are also able to demonstrate the beginning of the breakdown of the *LS* coupling for resonance series corresponding to electron configurations with higher orbital angular momenta and those above the third ionization threshold.

DOI: 10.1103/PhysRevA.80.042509 PACS number(s): 31.15.aj, 32.80.Fb, 32.80.Zb

I. INTRODUCTION

In principle, for heavier alkaline-earth-metal atoms, with a smaller energy separation between higher-excited autoionizing resonances and a more substantial spin-dependent interaction, one would expect a stronger mixing between different spin states and thus more complicated spectra. However, the earlier observed spectra [1–3] have shown that the resonance structures are, in fact, relatively smooth above the second ionization threshold compared with those between the first and second ionization thresholds [1–4], where the resonance decays only into one dominating ionization channel. The lack of complex resonance structure results primarily from a much faster decay rate, in the presence of multiple decay channels, with a broader total resonance width and substantial overlaps between neighboring resonances. As a result, when the incident photon energy is sufficiently high to excite electron into multiple-ionization channels, it is difficult to investigate the detailed structure of the overlapping doubly excited autoionization series based on the experimental spectra alone. A more in-depth understanding of the resonance structures would therefore require a detailed multielectron theoretical analysis, which includes explicitly the spin-dependent interactions, together with a good agreement between theoretical and experimental spectra.

It is the purpose of this paper to present such an investigation with a B-spline-based complex-rotation (BSCR) calculation [5], together with more recent absolute absorption experimental data, for the ionization spectra of Ca and Sr from the first ionization threshold up for an extended spectral region, including multiple-ionization channels. By taking advantage of the ability of the BSCR approach to estimate explicitly the spin mixing, we will demonstrate explicitly how the spin-dependent interaction affects the mixing of different spin states and, in particular, the breakdown of the *LS* coupling along various autoionization series as energy increases.

The presence of the doubly excited triplet autoionizing series in the photoabsorption spectra from the singlet ground state of Sr was already confirmed in a number of earlier experiments [4,6]. The detailed theoretical study of the heavier alkaline-earth-metal atoms, including the spin-orbit interaction, was first carried out by Kim and Greene [7], using the multichannel-quantum-defect techniques with a $jj-LS$ frame transformation for Ca, and by Aymar [8] with a similar approach for Sr. Subsequent works were extended to include spectra for heavier Ba and Ra with a jj-coupled eigenchannel R-matrix calculation [9]. A comprehensive review, including detailed comparison between calculated and observed spectra from an extensive collection of theoretical and experimental results, was later given by Aymar *et al.* [10]. In spite of the general qualitative agreement between the theory and experiment, only limited attempts were made to characterize in detail the individual autoionization series.

Details of the theoretical approach and the experimental procedure for the absolute photoabsorption cross-sections measurement employed in this study were already presented in [3,5]. In Sec. II, we will briefly outline the BSCR approach and the experimental procedure. Results and discussions based on this joint theoretical and experimental study will be presented in Sec. III. In particular, we will focus our discussion on the detailed characterization of the individual doubly excited autoionization series for an extended energy region.

II. THEORY AND EXPERIMENT

To identify the dominating electronic configuration for each resonance, the BSCR calculation is carried out with sets of J-dependent orthonormal atomic basis functions $\psi^{\Omega}_{n_1 l_1, n_2 l_2, \ldots}(\vec{r}_1, \vec{r}_2, \ldots)$, which are characterized by an electronic configuration $(n_1 l_1, n_2 l_2, \ldots)$ and a set of quantum numbers $\Omega \equiv (SLJM_J)$, where S, L, J, and M_J are the total spin, the total orbital angular momentum, the total angular

*051420@mail.fju.edu.tw

momentum, and its corresponding magnetic quantum number, respectively. The one-particle radial function representing an outgoing ionized electron of an open channel is defined by replacing the radius r with a complex variable $z=re^{-i\theta}$. In addition, a variational parameter β for each open channel is also introduced to modify the one-particle radial function as defined by Eq. (4) of [5].

In the first step of the BSCR calculation, with the variational parameters β properly determined following the procedure detailed in [5], the *nonrelativistic* complex Hamiltonian matrix is diagonalized to obtain a zeroth-order state wave function, which is the sum of the *bound* (i.e., all close channel j) and *continuum* (i.e., all open channel k) components, i.e.,

$$\phi_\mu^\Omega(\theta)=\sum_j C^{(SLJ)\mu}_{n'_j\ell'_jn_j\ell_j}\psi^\Omega_{n'_j\ell'_jn_j\ell_j}+\sum_k C^{(SLJ)\mu}_{n'_k\ell'_k\varepsilon_k\ell_k(\theta)}\psi^\Omega_{n'_k\ell'_k\varepsilon_k\ell_k(\theta,\beta_k)}. \tag{1}$$

The doubly excited resonances $|n_0\ell_0n_\mu\ell_\mu\rangle$ with an inner electron $n_0\ell_0$ are identified approximately by projecting the state function $\phi_\mu^\Omega(\theta)$ to its corresponding basis function $\psi^\Omega_{n_0\ell_0n_\nu\ell_\nu}$, i.e., by calculating the spectral density

$$\rho_\mu^{SLJ}=\sum_\nu |\langle\phi_\mu^\Omega(\theta)|\psi^\Omega_{n_0\ell_0n_\nu\ell_\nu}\rangle|^2=\sum_\nu |C^{(SLJ)\mu}_{n_0\ell_0n_\nu\ell_\nu}|^2. \tag{2}$$

In the second step of the BSCR calculation, a total Hamiltonian matrix is constructed with the sets of zeroth-order state wave functions given by Eq. (1) to include explicitly the spin-dependent interactions (e.g., the spin-orbit interaction). For each total angular momentum J, all allowed SL states are included in our calculation. Following the procedures detailed in [5], the complex energy eigenvalues $E_\mu=E^\mu_{res}-i\Gamma_\mu/2$, in terms of the resonance energy E^μ_{res} and the resonance width Γ_μ, are obtained by diagonalizing the new total Hamiltonian matrix. The corresponding state functions are given by the linear combination of $\phi_\nu^\Omega(\theta)$, i.e.,

$$\Phi_\mu^{JM}(\theta)=\sum_{S,L,\nu} C_\nu^{(SL)J\mu}\phi_\nu^\Omega(\theta). \tag{3}$$

The mixing of the spin states can be determined by the sum over the square of the appropriate expansion coefficients, i.e., $|C_\nu^{(SL)J\mu}|^2$.

The photoionization cross section $\sigma(E)$ from an initial state $\Phi_I^{J_IM_I}$ with an energy E_I is given by the imaginary part of the dynamic polarizability [11,12], i.e.,

$$\sigma_{EI}(E)=4\pi\alpha\frac{(\Delta E)^{\pi_\gamma}}{3g_I}\mathrm{Im}\left(\sum_\mu\sum_{q,M,M_I}\frac{\langle\Phi_I^{J_IM_I}|D_q^{[1]}|\Phi_\mu^{JM}(\theta)\rangle^2}{E_\mu(\theta)-E}\right), \tag{4}$$

where α is the fine-structure constant, $g_I=2J_I+1$ is the degree of degeneracy of the initial state I, $\Delta E=E-E_I$ is the transition energy, D is the dipole operator, and $\pi_\gamma=1$ and -1 for the dipole velocity and length approximations, respectively. The state function of the initial state $\Phi_I^{J_IM_I}$ is calculated with the procedure outlined in [5,13]. Explicit expressions for the calculation of the transition matrix $\langle\Phi_I^{J_IM_I}|D_q^{[1]}|\Phi_\mu^{JM}(\theta)\rangle$ are given in [5].

The experimental setup and the procedure for the absolute photoabsoprtion spectra measurement are detailed in [3,14]. Light source at the National Synchrotron Radiation Research Center in Taiwan was used as the continuum background. The column density of the alkaline-earth vapors in a heatpipe was determined by measuring simultaneously the pressure and the temperature profiles along the heatpipe (see, e.g., Fig. 2 of [3] for a typical heatpipe temperature-distribution profile). The total number of the Ar buffer gas particles inside the heatpipe was calibrated with care and kept at a constant for an extended temperature range in the absence of the alkaline earth (see, e.g., Fig. 4 of [3]). By carefully measuring the temperatures along the heatpipe after the alkaline-earth sample was placed in the heatpipe at increasing temperature, the column density was determined with an uncertainty of about 7%, following the procedure outlined in [3]. The absolute absorption cross sections were determined by measuring the ratio of the incident light and the attenuated light. The estimated uncertainty in absolute cross section is about 10–15 %.

III. RESULTS AND DISCUSSIONS

Between the first $4s$ and the second $3d$ ionization thresholds of Ca, we include in our BSCR calculation, following the LS coupling, all six odd-parity autoionization series, i.e., $3dnp(^{1,3}P,^3D)$, $3dnf(^{1,3}P,^3D)$, and the first member of the $4pns(^{1,3}P)$ series, which decay into the $4s\epsilon p(^{1,3}P)J=1$ ionization channels from the initial ground state. The optimized β values for both singlet and triplet P open channels are 0.45 and θ is stabilized at around -0.25 rad. At higher energies, between the $3d$ and $4p$ thresholds, there are eight $J=1$ ionizaion channels, i.e., $4s\epsilon p(^{1,3}P)$, $3d\epsilon' p(^{1,3}P,^3D)$, and $3d\epsilon' f(^{1,3}P,^3D)$ channels with five autoionization series, i.e., $4pnd(^{1,3}P,^3D)$ and $4pns(^{1,3}P)$ series. The optimized β values are 0.425 for all the singlet and triplet P open channels and 0.4 for the triplet D open channels. The stabilized θ value is -0.22 rad in this energy region. At even higher energies, above the $4p$ threshold, we focus our study on the identification of a few members of the doubly excited $5snp(^{1,3}P)$ and $4dnp(^3D,^{1,3}P)$ resonance series, which decay into the $4s\epsilon p(^{1,3}P)$, $3d\epsilon' p(^{1,3}P,^3D)$, $3d\epsilon' f(^{1,3}P,^3D)$, $4p\epsilon'' s(^{1,3}P)$, and $4p\epsilon'' d(^{1,3}P,^3D)$ ionization channels. With a stabilized value of $\theta=-0.25$ rad, a single optimized value of $\beta=0.4$ is used for all singlet and triplet P channels and $\beta=0.525$ for the triplet D channels.

Figure 1 compares the calculated Ca ground-state photoionization cross sections with the observed spectrum between the $4s$ and $3d$ thresholds. The theory agrees well with the experiment in general, except for the peak cross sections for the narrow $3dnp(^3P,^3D)$ and $3dnf(^{1,3}P,^3D)$ resonances, which are substantially lower than the calculated ones due to the limited experimental energy resolution. Figure 2 presents a more detailed comparisons between theory and experiment between 55 000 and 59 000 cm^{-1}. Our calculation shows clearly a substantial effect due to the configuration interaction on the $3d4f$ multiplet between 55 800 and 56 000 cm^{-1} and the $3d6p$ multiplet between 56 200 and 57 000 cm^{-1}. These two multiplets are also affected by the presence of the

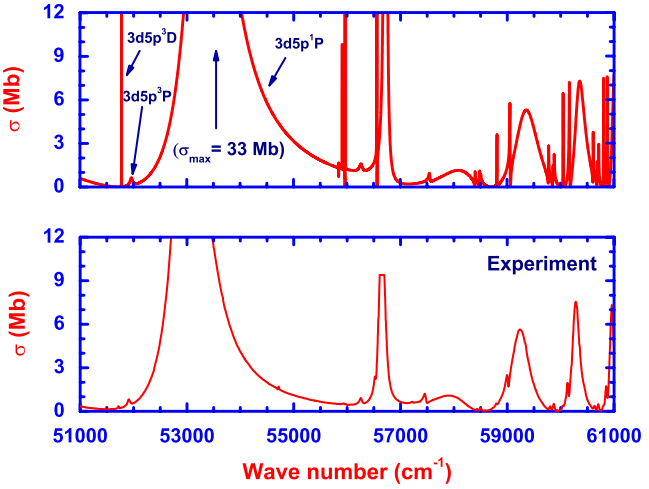

FIG. 1. (Color online) Comparison between the calculated Ca ground-state photoionization cross sections and the experimentally observed spectrum between the 4*s* and 3*d* thresholds.

$4p5s\ ^{1,3}P$ resonances between 57 400 and 58 400 cm^{-1}. In fact, for both multiplets, the two lower-energy levels are inverted, i.e., with ^3P below the ^3D resonance due to the stronger interaction between the $4p5s\ ^3P$ and $3d6p\ ^3P/3d4f\ ^3P$ resonances. This differs from the earlier assignment of the $3d6p\ ^3D$ state [1], which follows the Hund's rules with the $3d6p\ ^3D$ state below the $3d6p\ ^3P$ state. Each of the resonances in our calculation is identified in terms of their respective spectral densities corresponding to the mixing of different spin states listed in Table I. It is also interesting to note that the resonance width of the second member of the dominant $3dnp\ ^1P$ series (i.e., the one close to 56 600 cm^{-1} in the experimental spectrum shown in Fig. 1) is affected substantially by its interaction with the $4p5s\ ^{1,3}P$ resonances on the higher-energy side and is noticeably smaller than the third member (i.e., $3p7d\ ^1P$ close to 59 300 cm^{-1}) of the same series. The presence of the $4p5s\ ^{1,3}P$ resonances as the perturbers of the $3dnp$ and $3dnf$ autoionization series does

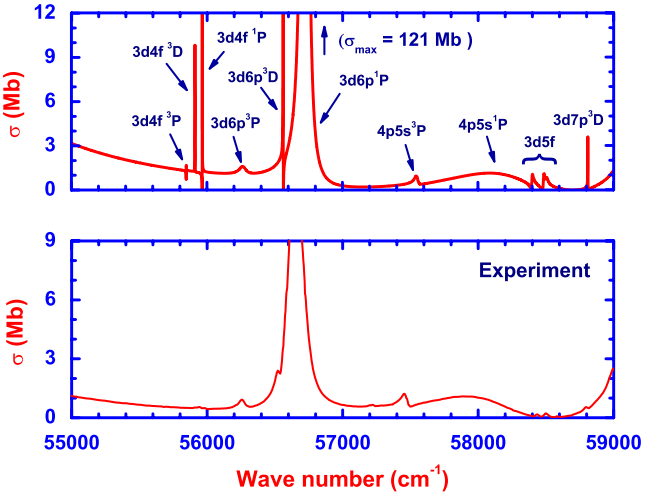

FIG. 2. (Color online) Detailed comparison between theory and experiment for spectrum shown in Fig. 1 from 55 000 to 59 000 cm^{-1}.

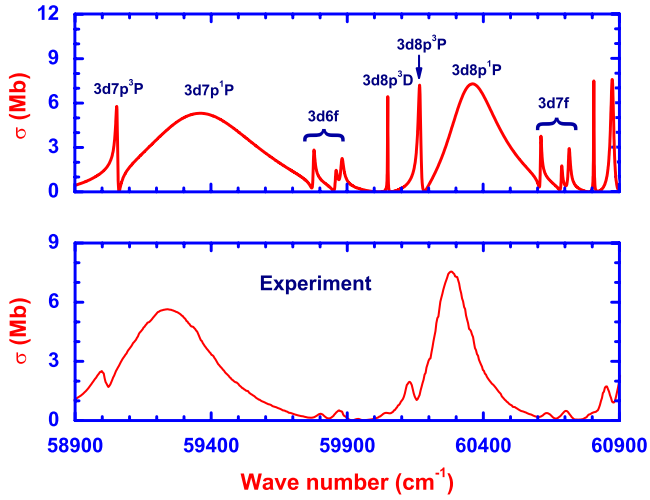

FIG. 3. (Color online) Detailed comparison between theory and experiment for spectrum shown in Fig. 1 from 58 900 to 60 900 cm^{-1}.

not affect the relative energies of the individual members of the $3dnp$ and $3dnf$ multiplets on the higher-energy side shown in Figs. 2 and 3 as the higher ^3P states are merely pushed up in energy by the perturbers.

Based on the spectral density of the spin states listed in Table I, it appears that all three $3dnp$ resonance series and also the two $4pns$ series could still be identified effectively in terms of the *LS* coupling. On the other hand, our calculation shows that, for resonance series corresponding to electron configurations with higher orbital angular momenta, such as the $3dnf$ series, the spectrum could no longer be represented by the *LS* coupling, especially for those members on the higher-energy side. Consequently, no specific spin state could be assigned to each resonance. However, based on our calculation, we do anticipate similar resonance structures for the $3d6f$ and $3d7f$ multiplets due to similar spectral densities corresponding to different spin states listed in Table I and, indeed, shown in Fig. 3.

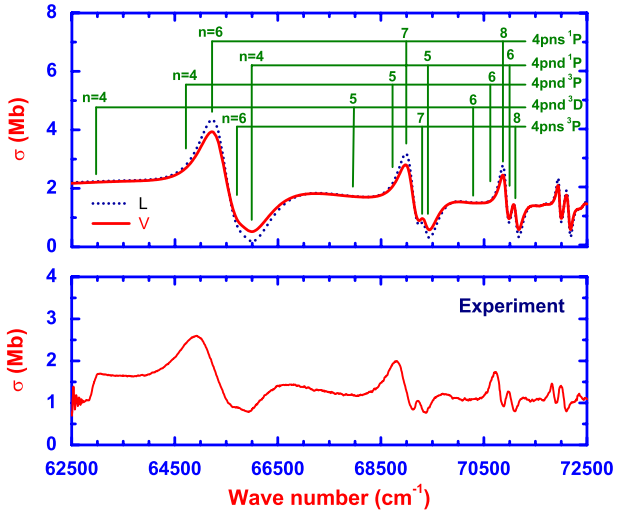

FIG. 4. (Color online) Comparison between the calculated Ca ground-state photoionization cross sections and the experimentally observed spectrum between the 3*d* and 4*p* thresholds.

TABLE I. The calculated resonance energies E_r (in Ry) with respect to the Ca double-ionization threshold, effective quantum numbers ν, widths Γ (in $a[n]=a\times 10^n$ Ry), and probability densities (in %) of selected $3dnp$, $3dnf$, and $4pns$ $^{1,3}L^o_{J=1}$ resonances.

State	E_r	ν	Γ	$^1P^o$	$^3P^o$	$^3D^o$
$3d5p\ ^3D^o$	−0.85033	3.12	4.4[−6]	4	5	91
$3d6p\ ^3D^o$	−0.80656	4.13	3.0[−6]	15	4	81
$3d7p\ ^3D^o$	−0.78599	5.12	1.5[−5]	10	7	83
$3d8p\ ^3D^o$	−0.77467	6.10	1.6[−5]	11	11	78
$3d5p\ ^3P^o$	−0.84870	3.15	7.8[−4]	5	91	4
$3d6p\ ^3P^o$	−0.80921	4.04	7.3[−4]	13	83	4
$3d7p\ ^3P^o$	−0.78372	5.28	7.4[−5]	18	77	5
$3d8p\ ^3P^o$	−0.77357	6.23	1.0[−4]	21	71	8
$3d5p\ ^1P^o$	−0.83637	3.36	6.8[−3]	94	4	2
$3d6p\ ^1P^o$	−0.80523	4.17	3.2[−4]	75	13	12
$3d7p\ ^1P^o$	−0.78131	5.46	4.6[−3]	86	9	5
$3d8p\ ^1P^o$	−0.77205	6.42	2.1[−3]	77	15	8
$3d4f\ ^3P^o$	−0.81295	3.92	8.6[−6]	26	47	27
$3d4f\ ^3D^o$	−0.81238	3.94	1.3[−5]	23	37	40
$3d4f\ ^1P^o$	−0.81186	3.95	2.6[−6]	56	8	36
$3d5f(1)$	−0.78968	4.89	1.0[−4]	36	20	44
$3d5f(2)$	−0.78889	4.93	1.1[−4]	42	21	37
$3d5f(3)$	−0.78869	4.95	1.7[−4]	37	59	4
$3d6f(1)$	−0.77711	5.84	6.6[−5]	33	22	45
$3d6f(2)$	−0.77637	5.92	8.0[−5]	30	33	37
$3d6f(3)$	−0.77617	5.94	1.3[−4]	47	45	8
$3d7f(1)$	−0.76950	6.79	4.7[−5]	31	22	47
$3d7f(2)$	−0.76880	6.90	5.9[−5]	24	37	39
$3d7f(3)$	−0.76855	6.94	9.1[−5]	46	43	11
$4p5s\ ^3P^o$	−0.79740	2.53	3.0[−4]	13	85	2
$4p5s\ ^1P^o$	−0.79136	2.58	9.1[−3]	83	12	5

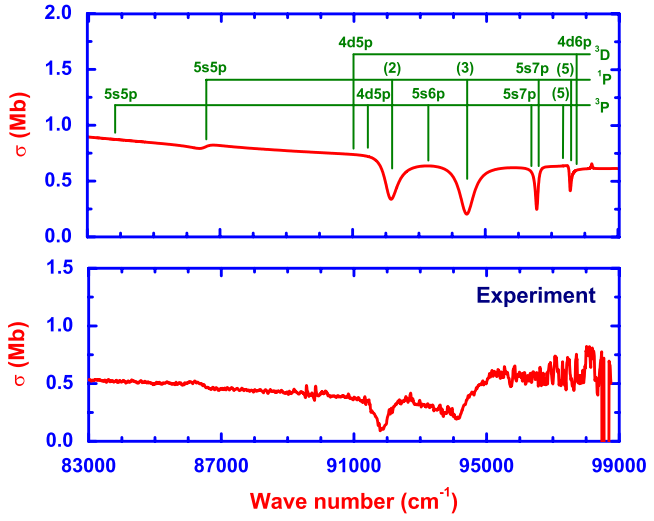

FIG. 5. (Color online) Comparison between the calculated Ca ground-state photoionization cross sections and the experimentally observed spectrum above the $4p$ threshold.

Figure 4 shows the calculated and observed spectra between the Ca^+3d and $4p$ thresholds. As expected, the resonance structures are dominated by the $4pns\ ^1P$ series. The "windowlike" structures are also known to have been identified as the $4pnd\ ^1P$ series. Table II shows substantial mixing between the three overlapping $4pns\ ^1P$, $4pns\ ^3P$, and $4pnd\ ^1P$ resonance series. In fact, the presence of the $4pnd\ ^1P$ series, with its strong configuration mixing with the $4pns\ ^1P$ series, has shifted the $4pns\ ^1P$ resonance to below the corresponding $4pns\ ^3P$ resonance, contrary to the Hund's rule. The singlet-triplet mixing due to the spin-orbit interaction has also led to the less prominent $4pns\ ^3P$ structures on the higher-energy shoulder of the $4pns\ ^1P$ resonance for higher n (e.g., $n=7-8$) states. Although the $4pnd(^3P,^3D)$ resonance series is hidden in the spectrum, the BSCR calculation is able to identify such series through the calculated resonance energies and widths, effective quantum numbers, and probability densities listed in Table II. In fact, they are hidden in part due to their relatively large resonance widths and also the relatively smaller transition amplitude. Our calculation also confirms, based on the calculated effective principal quantum number ν listed in Table II, that the first member of the $4pnd$ series above the $3d$ threshold is indeed the

TABLE II. The calculated resonance energies E_r (in Ry) with respect to the Ca double-ionization threshold, effective quantum numbers ν, widths Γ (in $a[n]=a\times 10^n$ Ry), and probability densities (in %) of selected $4pnd$ and $4pns$ $^{1,3}L^o_{J=1}$ resonances.

State	E_r	ν	Γ	$^1P^o$	$^3P^o$	$^3D^o$
$4p4d\ ^3D^o$	−0.74723	3.07	1.5[−2]	9	5	86
$4p5d\ ^3D^o$	−0.70212	4.06	6.7[−3]	13	9	78
$4p6d\ ^3D^o$	−0.68060	5.05	3.1[−3]	20	13	67
$4p7d\ ^3D^o$	−0.66891	6.02	1.9[−3]	28	17	55
$4p4d\ ^3P^o$	−0.73122	3.34	1.7[−2]	6	90	4
$4p5d\ ^3P^o$	−0.69584	4.28	9.4[−3]	9	83	8
$4p6d\ ^3P^o$	−0.67735	5.27	4.8[−3]	13	73	14
$4p7d\ ^3P^o$	−0.66675	6.28	2.8[−3]	17	64	19
$4p4d\ ^1P^o$	−0.72104	3.54	1.5[−2]	82	14	4
$4p5d\ ^1P^o$	−0.68956	4.55	7.4[−3]	71	22	7
$4p6d\ ^1P^o$	−0.67387	5.55	4.2[−3]	61	29	10
$4p7d\ ^1P^o$	−0.66483	6.53	2.7[−3]	55	32	13
$4p6s\ ^1P^o$	−0.72628	3.43	7.0[−3]	81	16	3
$4p7s\ ^1P^o$	−0.69235	4.43	3.6[−3]	68	27	5
$4p8s\ ^1P^o$	−0.67560	5.40	1.5[−3]	60	34	6
$4p6s\ ^3P^o$	−0.72181	3.53	3.6[−3]	21	79	0
$4p7s\ ^3P^o$	−0.69004	4.53	2.1[−3]	35	63	2
$4p8s\ ^3P^o$	−0.67382	5.55	1.6[−3]	47	49	4

$4p4d$ state, as suggested earlier by Scott *et al.* [15]. The length and velocity results from our calculation are in good agreement, as shown in Fig. 4.

Figure 5 compares the calculated photoionization and the observed photoabsorption spectra from the ground state of Ca above the Ca^+4p threshold. The resonance structures are dominated by the window-type ^1P resonances. The agreement between the theory and experiment is generally good up to 95 000 cm^{-1}. Above 95 000 cm^{-1}, the measurement could no longer resolve the spectrum. The calculated resonance energies and widths, effective quantum numbers, and probability densities are presented in Table III. Although all the states listed in Table III could be identified by their dominant spin states, the strong configuration mixing has shown another feature in the breakdown of the *LS* coupling. For example, from a closed-channel calculation for the ^3P symmetry, our calculation has shown a strong configuration mixing for the fifth [i.e., $^3P^o(5)$] resonance state, between the

TABLE III. The calculated resonance energies E_r (in Ry) with respect to the Ca double-ionization threshold, effective quantum numbers ν_{nl} against the nl threshold, widths Γ (in $a[n]=a\times 10^n$ Ry), and probability densities (in %) of selected $5snp$ and $4dnp$ $^{1,3}L^o_{J=1}$ resonances.

State	E_r	ν_{nl}	Γ	$^1P^o$	$^3P^o$	$^3D^o$
$5s5p\ ^3P^o$	−0.55931	2.48_{5s}	2.4[−3]	4	95	1
$4d5p\ ^3P^o$	−0.48900	2.69_{4d}	6.0[−3]	3	93	4
$5s6p\ ^3P^o$	−0.47228	3.63_{5s}	8.2[−4]	3	96	1
$5s7p\ ^3P^o$	−0.44249	4.67_{5s}	2.4[−4]	7	92	1
$^3P^o(5)$	−0.43488	$5.11_{5s}/3.44_{4d}$	2.5[−4]	9	88	3
$5s8p\ ^3P^o$	−0.42755	5.68_{5s}	1.7[−4]	5	94	1
$5s5p\ ^1P^o$	−0.53334	2.70_{5s}	4.6[−3]	95	3	2
$^1P^o(2)$	−0.48239	$3.41_{5s}/2.75_{4d}$	4.2[−3]	94	4	2
$^1P^o(3)$	−0.46130	$3.93_{5s}/3.01_{4d}$	4.7[−3]	96	3	1
$5s7p\ ^1P^o$	−0.44194	4.69_{5s}	9.1[−4]	91	8	1
$^1P^o(5)$	−0.43284	$5.25_{5s}/3.49_{4d}$	5.5[−4]	84	8	8
$5s8p\ ^1P^o$	−0.42686	5.74_{5s}	3.6[−4]	94	5	1
$4d5p\ ^3D^o$	−0.49224	2.66_{4d}	7.4[−3]	5	4	91
$4d6p\ ^3D^o$	−0.43179	3.51_{4d}	2.0[−4]	10	3	87

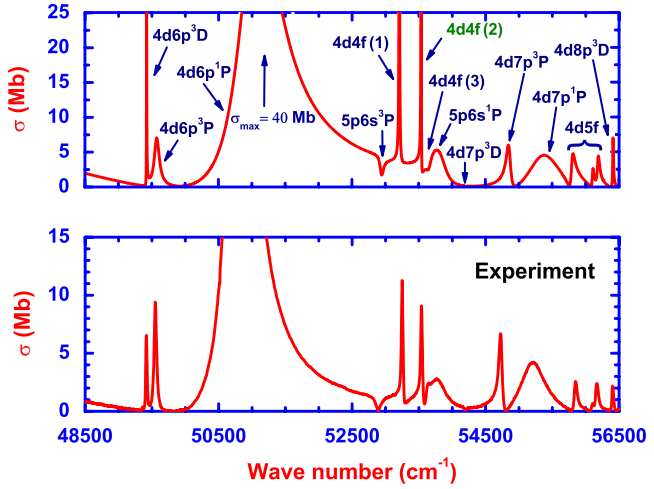

FIG. 6. (Color online) Comparison between the calculated Sr ground-state photoionization cross sections and the experimentally observed spectrum between the 5*s* and 4*d* thresholds.

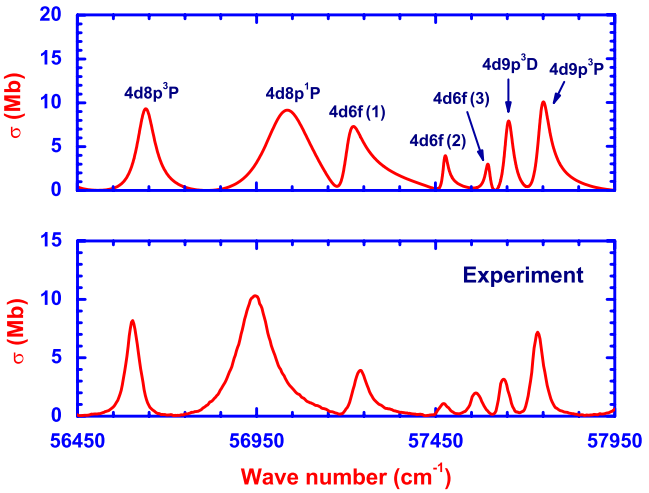

FIG. 7. (Color online) Detailed comparison between theory and experiment for spectrum shown in Fig. 6 from 56 450 to 57 950 cm^{-1}.

$4dnp$ (44%), $4dnf$ (19%), and $5pns$ (29%) series. We have listed its effective quantum numbers against both the Ca^+5s and $4d$ thresholds. It is by no means without ambiguity, but, one might still nominally designate this state as the $4d6p\ ^3P$ state since its effective principle quantum number against the $4d$ threshold, i.e., $\nu_{4d}=3.44$, is more in line with the effective principle quantum number of $\nu_{4d}=2.69$ of the $4d5p\ ^3P$ state. In fact, this state could hardly be fitted into the $5snp\ ^3P$ series based on its effective principle quantum number against the $5s$ threshold at $\nu_{5s}=5.11$. Similar closed-channel calculation for the ^1P symmetry shows that the dominant configurations for the $^1P(2)$ state consist of the $5snp$ (56%) and $4dnp$ (28%) series. For the $^1P(3)$ state, the dominant configurations include $5snp$ (63%), $4dnp$ (16%), and $4dnf$

TABLE IV. The calculated resonance energies E_r (in Ry) with respect to the Sr double-ionization threshold, effective quantum numbers ν, widths Γ (in $a[n]=a\times 10^n$ Ry), and probability densities (in %) of selected $4dnp$, $4dnf$, and $5p6s\ ^{1,3}L^o_{J=1}$ resonances.

State	E_r	ν	Γ	$^1P^o$	$^3P^o$	$^3D^o$
$4d6p\ ^3D^o$	−0.77888	3.12	5.1[−5]	12	11	77
$4d7p\ ^3D^o$	−0.73539	4.12	2.0[−4]	20	13	67
$4d8p\ ^3D^o$	−0.71520	5.08	1.3[−4]	18	18	64
$4d9p\ ^3D^o$	−0.70390	6.04	2.8[−4]	24	31	45
$4d6p\ ^3P^o$	−0.77752	3.15	8.2[−4]	16	74	10
$4d7p\ ^3P^o$	−0.72936	4.35	7.2[−4]	31	61	8
$4d8p\ ^3P^o$	−0.71313	5.22	5.6[−4]	32	54	14
$4d9p\ ^3P^o$	−0.70305	6.13	3.6[−4]	28	46	26
$4d6p\ ^1P^o$	−0.76439	3.37	6.8[−3]	75	16	9
$4d7p\ ^1P^o$	−0.72506	4.54	5.8[−3]	58	26	16
$4d8p\ ^1P^o$	−0.70961	5.49	1.6[−3]	51	27	22
$4d4f(1)$	−0.74437	3.84	1.1[−4]	37	24	39
$4d5f(1)$	−0.72082	4.75	5.4[−4]	35	23	42
$4d6f(1)$	−0.70799	5.63	4.8[−4]	36	23	41
$4d4f(2)$	−0.74139	3.92	3.2[−5]	43	15	42
$4d5f(2)$	−0.71797	4.91	2.6[−4]	24	36	40
$4d6f(2)$	−0.70552	5.87	1.6[−4]	21	38	41
$4d4f(3)$	−0.74025	3.96	8.6[−4]	35	54	11
$4d5f(3)$	−0.71724	4.95	3.8[−4]	43	42	15
$4d6f(3)$	−0.70439	5.98	1.6[−4]	43	31	26
$5p6s\ ^3P^o$	−0.74683	2.52	5.8[−4]	27	65	8
$5p6s\ ^1P^o$	−0.73865	2.59	2.7[−3]	51	34	15

(16%) series, and for the $^1P(5)$ state, the $5snp$ (19%), $4dnp$ (45%), $4dnf$ (15%), and $5pns$ (17%) series. Again, we list in Table III for those three states the effective quantum numbers ν against both the Ca^+5s and $4d$ thresholds. One might be able to designate two of these three states, e.g., $^1P(2)$ and $^1P(5)$ as the $4d5p\ ^1P$ and $4d6p\ ^1P$ states, respectively, and the $^1P(3)$ state as the $5s6p\ ^1P$ resonance; but, it would be nothing more than semantics than an accurate physical interpretation.

For Sr, between the first $5s$ and second $4d$ ionization thresholds, our study includes all six odd-parity autoionization series, i.e., $4dnp(^{1,3}P,^3D)$, $4dnf(^{1,3}P,^3D)$, and the first member of the $5pns(^{1,3}P)$ series, which decay into the $5s\epsilon p(^{1,3}P)J=1$ ionization channel from the initial ground state. The optimized β values for singlet and triplet P open channels are 0.25 and 0.30, respectively, and θ is stabilized at around -0.2 rad. Between the $4d$ and $5p$ thresholds, there are eight $J=1$ ionizaion channels, i.e., $5s\epsilon p(^{1,3}P)$, $4d\epsilon' p(^{1,3}P,^3D)$ and $4d\epsilon' f(^{1,3}P,^3D)$ channels with five autoionization series, i.e., $5pnd(^{1,3}P,^3D)$ and $5pns(^{1,3}P)$ series. For singlet and triplet P open channels, their optimized β values are 0.5 and 0.35, respectively, and for the triplet D open channels, β is 0.375. The stabilized value of θ is -0.2 rad in this energy region. Above the $5p$ threshold, we have investigated a few members of the doubly excited $6snp(^{1,3}P)$ and $5dnp(^3D,^{1,3}P)$ resonance series, which decay into the $5s\epsilon p(^{1,3}P)$, $4d\epsilon' p(^{1,3}P,^3D)$, $4d\epsilon' f(^{1,3}P,^3D)$, $5p\epsilon'' s(^{1,3}P)$, and $5p\epsilon'' d(^{1,3}P,^3D)$ ionization channels. Together with a stabilized value of $\theta=-0.2$ rad in this extended region, the singlet P channels have an optimized value of $\beta=0.4$, the triplet P channels $\beta=0.44$, and the triplet D channels $\beta=0.525$.

Figures 6 and 7 show good agreement between the calculated ground-state photoionization cross sections and the measured photoabsorption spectra between the $5s$ and $4d$ thresholds. The calculated resonance energies and widths, effective quantum numbers, and probability densities are tabulated in Table IV. Unlike the level inversion for the $3d6p$ and $3d4f$ multiplets for Ca discussed earlier, the relative energy levels for the $4d6p$ multiplet follow the Hund's rules, i.e., they are not affected by the presence of the $5p6s\ ^{1,3}P$ resonances, which overlap substantially with the $4d4f$ multiplet between 52 500 and 54 000 cm^{-1}. Again, our calculation has shown the breakdown of the LS coupling with strong mixing of different spin states for all $4dnf$ series, which is similar to the $3dnf$ series of Ca. Another interesting question

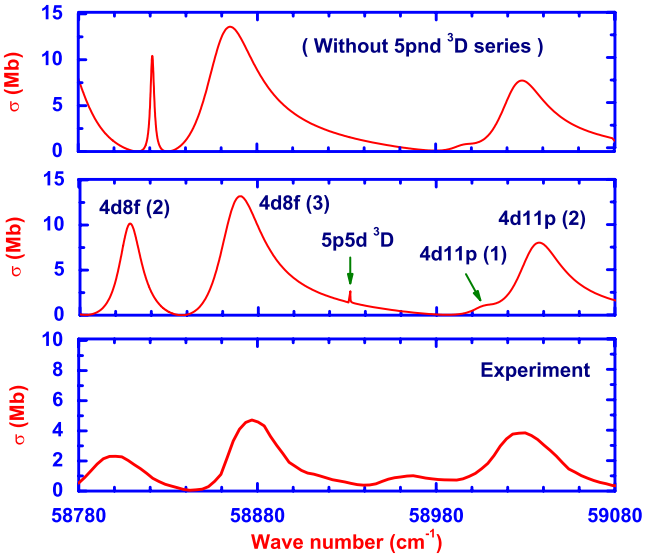

FIG. 8. (Color online) Comparison between the calculated Sr ground-state photoionization cross sections and the experimentally observed spectrum in the vicinity of the $5p5d\ ^3D$ state. The top graph was calculated with the $5pnd\ ^3D$ series excluded.

is about the location of the first member of the $5pnd\ ^3D$ series. According to the earlier studies, the $5p5d$ levels are completely embedded in several resonances [8] and are broadly distributed around 58 000 cm^{-1} to 59 000 cm^{-1} (see Fig. 2 in [2]). However, our calculation has shown that the $5p5d\ ^3D$ state actually falls below the $4d$ threshold, as shown in Fig. 8. The $5p5d\ ^3D$ resonance in the theoretically calculated BSCR spectrum close to 58 930 cm^{-1} shown in the middle graph of Fig. 8 could be unambiguously identified when compared with the top graph in Fig. 8, which was obtained by excluding the $5pnd\ ^3D$ series in our calculation. Although this resonance is not observed in the experimental spectrum (see, e.g., the bottom graph of Fig. 8) due to the lack of energy resolution, our calculation has led to a $5p5d\ ^3D$ state with spectral densities of 31% singlet P, 23% triplet P, and 46% triplet D (see Table V). Its effective quantum number of 3.11 against the $5p$ threshold is also consistent with that of the other members of the $5pnd\ ^3D$ series (i.e., 4.13 for the $5p6d\ ^3D$ and 5.07 for the $5p7d\ ^3D$ states) listed in Table VI.

Between the Sr^+4d and $5p$ thresholds, the spectrum is dominated by the $5pns\ ^{1,3}P$ resonances, as shown in Fig. 9, where the agreement of the structure profiles between the

TABLE V. The effective quantum numbers ν_{nl} against the nl threshold and probability densities (in %) of the five resonances based on the BSCR calculation shown in Fig. 8. The state is nominally identified by the B-spline-based configuration-interation (BSCI) calculation with closed channels only.

State	ν_{nl}	$^1P^o$	$^3P^o$	$^3D^o$	Assignment
$4d8f\ ^3P^o$	7.69_{4d}	30	40	30	$4d8f(2)$
$4d8f\ ^1P^o$	7.81_{4d}	37	35	28	$4d8f(3)$
$5p5d\ ^3D^o$	3.11_{5p}	31	23	46	$5p5d\ ^3D^o$
$4d11p\ ^3D^o$	8.14_{4d}	29	45	26	$4d11p(1)$
$4d11p\ ^3P^o$	8.21_{4d}	31	31	38	$4d11p(2)$

TABLE VI. The calculated resonance energies E_r (in Ry) with respect to the Sr double-ionization threshold, effective quantum numbers ν, widths Γ (in $a[n]=a\times 10^n$ Ry), and probability densities (in %) of selected $5pnd$ and $5pns$ $^{1,3}L^o_{J=1}$ resonances.

State	E_r	ν	Γ	$^1P^o$	$^3P^o$	$^3D^o$
$5p6d\ ^3D^o$	−0.64777	4.13	7.5[−3]	29	16	55
$5p7d\ ^3D^o$	−0.62793	5.07	3.9[−3]	35	20	45
$5p5d\ ^3P^o$	−0.66919	3.53	1.4[−2]	17	68	15
$5p6d\ ^3P^o$	−0.63868	4.49	8.0[−3]	20	61	19
$5p7d^3P^o$	−0.62207	5.51	3.9[−3]	29	45	26
$5p5d\ ^1P^o$	−0.66263	3.69	9.6[−3]	59	27	14
$5p6d\ ^1P^o$	−0.63417	4.71	4.8[−3]	53	30	17
$5p7d\ ^1P^o$	−0.62007	5.68	3.1[−3]	47	35	18
$5p7s\ ^3P^o$	−0.67167	3.48	3.1[−3]	48	45	7
$5p8s\ ^3P^o$	−0.64058	4.41	1.4[−3]	48	46	6
$5p9s\ ^3P^o$	−0.62489	5.29	8.4[−4]	47	46	7
$5p7s\ ^1P^o$	−0.66698	3.58	4.3[−3]	47	48	5
$5p8s\ ^1P^o$	−0.63557	4.64	2.3[−3]	50	42	8
$5p9s\ ^1P^o$	−0.61957	5.73	9.3[−4]	51	36	13

theory and experiment is generally good. Since the spin-orbit interaction is much stronger in Sr than in Ca, the mixing ratio between the $4pns\ ^3P$ states and the $4pns\ ^1P$ states is close to one as listed in Table VI. As a result, the $5pns\ ^3P$ series is as prominent as that of the $5pns\ ^1P$ series. Whereas the $5pnd\ ^3D$ series is largely hidden in the spectrum, the $5pnd\ ^{1,3}P$ series are located in the valleys between peaks of their neighboring $5pns$ states. Table VI lists the calculated resonance energies and widths, effective quantum numbers, and probability densities for the $5pn\ell(^{1,3}P,^3D)$ series. Similar to Ca, Fig. 9 shows good agreement between the length and velocity results from our calculation.

The calculated and the measured spectra above the $5p$ threshold for Sr are shown in Fig. 10, where the resonance structure is dominated by the window-type ^1P resonances. Similar to our study of the Ca spectrum above the $4p$ threshold, we have carried out a closed-channel calculation for the ^3P symmetry, which shows a strong configuration mixing between the $5dnp$ (38%), $5dnf$ (18%), and $6pns$ (37%) series for the fifth $^3P(5)$ resonance. A closed-channel calculation for the ^1P symmetry shows that the dominant configurations for the $^1P(2)$ state consist of the $6snp$ (55%) and $5dnp$ (26%) series. The dominant configurations for the $^1P(3)$ state include the $6snp$ (61%), $5dnp$ (14%), and $5dnf$ (20%) series, and for the $^1P(5)$ state, the $6snp$ (37%), $5dnp$ (27%), $5dnf$ (12%), and $6pns$ (21%) series. We have listed in Table VII the effective quantum numbers of these diluted states against both the Sr^+6s and $5d$ thresholds. One might be able to identify one or two of those states with the $5dnp\ ^{1,3}P$ series. But,

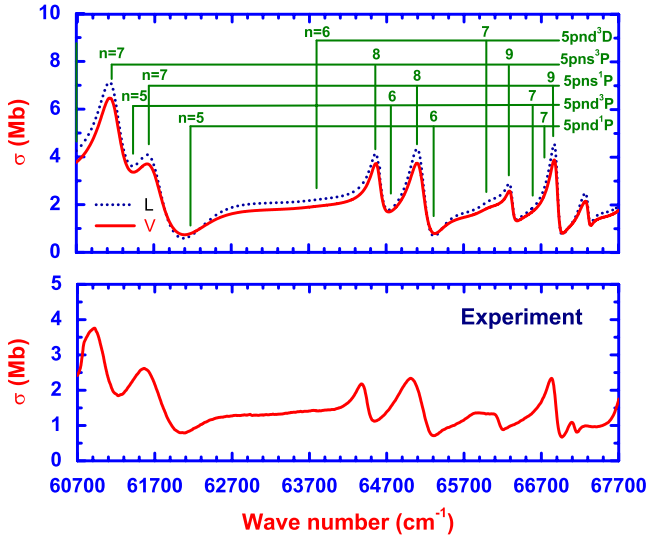

FIG. 9. (Color online) Comparison between the calculated Sr ground-state photoionization cross sections and the experimentally observed spectrum between the $4d$ and $5p$ thresholds.

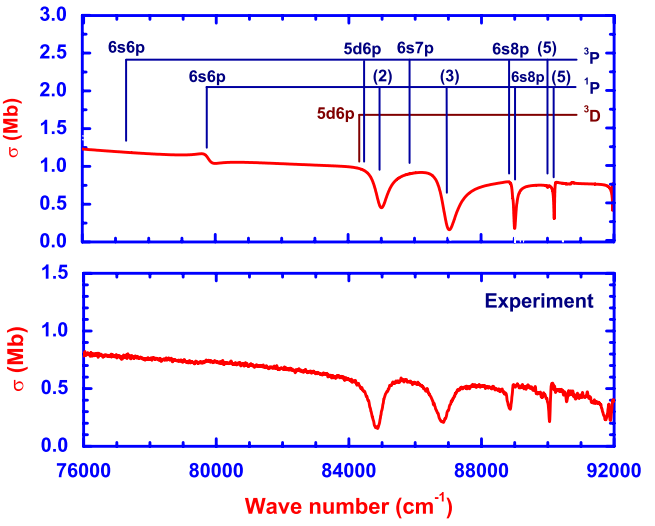

FIG. 10. (Color online) Comparison between the calculated Sr ground-state photoionization cross sections and the experimentally observed spectrum above the $5p$ threshold.

TABLE VII. The calculated resonance energies E_r (in Ry) with respect to the Sr double-ionization threshold, effective quantum numbers ν_{nl} against the nl threshold, widths Γ (in $a[n]=a\times 10^n$ Ry), and probability densities (in %) of selected $6snp$ and $5dnp$ $^{1,3}L^o_{J=1}$ resonances.

State	E_r	ν_{nl}	Γ	$^1P^o$	$^3P^o$	$^3D^o$
$6s6p\ ^3P^o$	−0.52539	2.58_{6s}	2.7[−3]	13	85	2
$5d6p\ ^3P^o$	−0.45927	2.71_{5d}	5.9[−3]	6	68	26
$6s7p\ ^3P^o$	−0.44647	3.73_{6s}	7.9[−4]	11	87	2
$6s8p\ ^3P^o$	−0.41863	4.77_{6s}	3.2[−4]	24	74	2
$^3P^o(5)$	−0.40900	$5.39_{6s}/3.41_{5d}$	2.6[−4]	27	67	6
$6s9p\ ^3P^o$	−0.40444	5.79_{6s}	2.0[−4]	11	87	2
$6s6p\ ^1P^o$	−0.50217	2.80_{6s}	3.4[−3]	83	11	6
$^1P^o(2)$	−0.45495	$3.53_{6s}/2.75_{5d}$	4.1[−3]	78	13	9
$^1P^o(3)$	−0.43671	$4.01_{6s}/2.96_{5d}$	4.7[−3]	87	9	4
$6s8p\ ^1P^o$	−0.41821	4.79_{6s}	8.0[−4]	72	26	2
$^1P^o(5)$	−0.40724	$5.54_{6s}/3.44_{5d}$	2.7[−4]	69	24	7
$6s9p\ ^1P^o$	−0.40249	5.99_{6s}	5.0[−4]	75	13	12
$5d6p\ ^3D^o$	−0.46019	2.70_{5d}	6.0[−3]	15	24	61
$5d7p\ ^3D^o$	−0.40398	3.51_{5d}	2.3[−4]	21	8	71

based on our study, it merely shows once again the beginning of the breakdown of the *LS* coupling as we discussed earlier.

By including explicitly the configuration interactions and the spin-dependent interactions, the theoretical Ca and Sr spectra for the overlapping resonance series presented in this paper offer detailed interpretations of the atomic transitions as energy increases across successive ionization thresholds. The proposed interpretations are supported by the good agreement between theory and experiment. In particular, our study has identified the inversion of energy levels of a number of multiplets as the results of strong configuration interactions due to the presence of perturbers from other overlapping resonance series. In addition, we have demonstrated the breakdown of *LS* coupling due to the spin mixing for resonance series corresponding to electron configuration with higher orbital angular momenta, such as the $3dnf$ series between the first and second ionization thresholds for Ca and the $4dnf$ series between the first and second ionization thresholds for Sr. The strong configuration interactions are also responsible for the breakdown of *LS* coupling for a number of doubly excited resonance series at higher energy, such as those above the $4p$ threshold for Ca and those above the $5p$ threshold for Sr.

ACKNOWLEDGMENT

This work was supported by the National Science Council in Taiwan under the Grant Nos. NSC 95-2112-M-030-004, NSC 96-2112-M-008-010-MY3, and NSC 98-2119-M-007-001.

[1] U. Griesmann, N. Shen, J. P. Connerade, K. Sommer, and J. Hormes, J. Phys. B **21**, L83 (1988).
[2] U. Griesmann, B. Esser, and J. Hormes, J. Phys. B **27**, 3939 (1994).
[3] C. C. Chu, H. S. Fung, H. H. Wu, and T. S. Yih, J. Phys. B **31**, 3843 (1998).
[4] R. D. Hudson, V. L. Carter, and P. A. Young, Phys. Rev. **180**, 77 (1969).
[5] T. K. Fang and T. N. Chang, Phys. Rev. A **76**, 012721 (2007).
[6] W. R. S. Garton and K. Codling, Proc. Phys. Soc. London **75**, 87 (1960); **86**, 1067 (1965); J. Phys. B **1**, 106 (1968).
[7] L. Kim and C. H. Greene, Phys. Rev. A **36**, 4272 (1987); **38**, 2361 (1988).
[8] M. Aymar, J. Phys. B **20**, 6507 (1987).
[9] C. H. Greene and M. Aymar, Phys. Rev. A **44**, 1773 (1991).
[10] M. Aymar, C. H. Greene, and E. Luc-Koenig, Rev. Mod. Phys. **68**, 1015 (1996).
[11] U. Fano and J. W. Cooper, Rev. Mod. Phys. **40**, 441 (1968).
[12] H. P. Kelly and A. Ron, Phys. Rev. A **5**, 168 (1972).
[13] T. N. Chang, in *Many-body Theory of Atomic Structure and Photoionization*, edited by T. N. Chang (World Scientific, Singapore, 1993), p. 213.
[14] M. Aymar, J.-M. Lecomte, C. C. Chu, H. S. Fung, H. H. Wu, and T. S. Yih, J. Phys. B **31**, 5135 (1998).
[15] P. Scott, A. E. Kingston, and A. Hibbert, J. Phys. B **16**, 3945 (1983).